Inorganic Chemistry
Article

Inorg. Chem. **2011**, *50*, 309–316 **309**
DOI: 10.1021/ic101948q

Flexible Mixed-Spin Kagomé Coordination Polymers with Reversible Magnetism Triggered by Dehydration and Rehydration

Wei-Xiong Zhang, Wei Xue, and Xiao-Ming Chen*

MOE Key Laboratory of Bioinorganic and Synthetic Chemistry/State Key Laboratory of Optoelectronic Materials and Technologies, School of Chemistry and Chemical Engineering, Sun Yat-Sen University, Guangzhou 510275, China

Received September 23, 2010

Two new two-dimensional (2D) heterometal coordination polymers $[Cu_2M(tzdc)_2(H_2O)_2]\cdot 2H_2O$ [M = Fe^{2+} (**1**) or Mn^{2+} (**2**); $tzdc^{3-}$ = 1,2,3-triazole-4,5-dicarboxylate] were assembled by using the $tzdc^{3-}$, Cu^{2+}, and Fe^{2+}/Mn^{2+} ions. Single-crystal X-ray analysis reveals that the two compounds consist of mixed-spin microporous Kagomé layers, which are packed into three-dimensional structures by hydrogen bonding and interlayer weak Cu···O interactions. When heated, they can release in a stepwise manner the uncoordinated and coordinated water molecules to produce dehydrated phases (**1′** and **2′**), respectively, which are stable up to ∼300 °C. The structures of **1′** and **2′** were determined by powder X-ray diffraction analysis, which reveals a change in the coordination sphere of Fe^{2+}/Mn^{2+} ions from an octahedron to an elongated 4+2 form, and a microporous-to-nonporous structural transformation involving intralayer wrinkling and interlayer superimposition. When the dehydrated samples are exposed to air, they can return to the hydrated phases quickly by adsorption of water molecules. Accordingly, a reversible change in magnetism between the ferrimagnetic character of the hydrated samples and the suppressed ferrimagnetic character of the dehydrated samples was found in this reversible dehydration and rehydration. These facts indicate these 2D heterometal coordination polymers are unique flexible 2D dynamic magnetic materials.

Introduction

Dynamic materials possessing a reversible change in magnetic properties in the solid state have attracted increasing interest over the past decade, because of their potential application as switches or sensors.[1−3] The porous coordination polymers are an attractive approach for this purpose, as their versatile pores provide possibilities for reversible modulation on the coordination sphere of the magnetic ion via the change in local host−guest interaction[2] and/or release and exchange of coordinated molecules.[3] In particular, the two-dimensional (2D) microporous coordination polymers are favorable candidates, because they can potentially adopt changes either within the layer or between the layers in response to external stimuli.[4−8] Among them, the Kagomé network is a special one, as it not only belongs to an important 2D magnetic topology that usually exhibits the fascinating spin-frustration magnetism but also potentially

*To whom correspondence should be addressed. Fax: (86)-20-84112245. Phone: (86)-20-84112074. E-mail: cxm@mail.sysu.edu.cn.

(1) (a) Kahn, O.; Larionova, J.; Yakhmi, J. V. *Chem.—Eur. J.* **1999**, *5*, 3443. (b) Niel, V.; Thompson, A. L.; Muñoz, M. C.; Galet, A.; Goeta, A. E.; Real, J. A. *Angew. Chem., Int. Ed.* **2003**, *42*, 3760. (c) Kurmoo, M.; Kumagai, H.; Akita-Tanaka, M.; Inoue, K.; Takagi, S. *Inorg. Chem.* **2006**, *45*, 1627. (d) Cheng, X.-N.; Zhang, W.-X.; Chen, X.-M. *J. Am. Chem. Soc.* **2007**, *129*, 15738. (e) Kaneko, W.; Ohba, M.; Kitagawa, S. *J. Am. Chem. Soc.* **2007**, *129*, 13706. (f) Zhang, Y.-J.; Liu, T.; Kanegawa, S.; Sato, O. *J. Am. Chem. Soc.* **2009**, *131*, 7942. (g) Duan, Z.-M.; Zhang, Y.; Zhang, B.; Zhu, D.-B. *J. Am. Chem. Soc.* **2009**, *131*, 6934. (h) Yoshida, Y.; Inoue, K.; Kurmoo, M. *Inorg. Chem.* **2009**, *48*, 10726. (i) Zhuang, W.-J.; Sun, H.-L.; Xu, H.-B.; Wang, Z.-M.; Gao, S.; Jin, L.-P. *Chem. Commun.* **2010**, *46*, 4339. (j) Motokawa, N.; Matsunaga, S.; Takaishi, S.; Miyasaka, H.; Yamashita, M.; Dunbar, K. R. *J. Am. Chem. Soc.* **2010**, *132*, 11943.

(2) (a) Maspoch, D.; Ruiz-Molina, D.; Wurst, K.; Domingo, N.; Cavallini, M.; Biscarini, F.; Tejada, J.; Rovira, C.; Veciana, J. *Nat. Mater.* **2003**, *2*, 190. (b) Kurmoo, M.; Kumagai, H.; Hughes, S. M.; Kepert, C. J. *Inorg. Chem.* **2003**, *42*, 6709. (c) Wang, Z.-M.; Zhang, B.; Fujiwara, H.; Kobayashi, H.; Kurmoo, M. *Chem. Commun.* **2004**, 416. (d) Kurmoo, M.; Kumagai, H.; Chapmanc, K. W.; Kepert, C. J. *Chem. Commun.* **2005**, 3012. (e) Zeng, M.-H.; Feng, X.-L.; Zhang, W.-X.; Chen, X.-M. *Dalton Trans.* **2006**, 5294. (f) Zhang, X.-M.; Hao, Z.-M.; Zhang, W.-X.; Chen, X.-M. *Angew. Chem., Int. Ed.* **2007**, *46*, 3456. (g) Wang, X.-Y.; Scancella, M.; Sevov, S. C. *Chem. Mater.* **2007**, *19*, 4506. (h) Halder, G. J.; Kepert, C. J.; Moubaraki, B.; Murray, K. S.; Cashion, J. D. *Science* **2002**, *298*, 1762. (i) Southon, P. D.; Liu, L.; Fellows, E. A.; Price, D. J.; Halder, G. J.; Chapman, K. W.; Moubaraki, B.; Murray, K. S.; Létard, J.-F.; Kepert, C. J. *J. Am. Chem. Soc.* **2009**, *131*, 10998.

(3) (a) Galet, A.; Muñoz, M. C.; Real, J. A. *Chem. Commun.* **2006**, 4321. (b) Cheng, X.-N.; Zhang, W.-X.; Lin, Y.-Y.; Zheng, Y.-Z.; Chen, X.-M. *Adv. Mater.* **2007**, *19*, 1494. (c) Milon, J.; Daniel, M. C.; Kaiba, A.; Guionneau, P.; Brandès, S.; Sutter, J. P. *J. Am. Chem. Soc.* **2007**, *129*, 13872.

(4) (a) Kitagawa, S.; Kitaura, R.; Noro, S.-i. *Angew. Chem., Int. Ed.* **2004**, *43*, 2334. (b) Kitagawa, S.; Uemura, K. *Chem. Soc. Rev.* **2005**, *34*, 109. (c) Férey, G.; Serre, C. *Chem. Soc. Rev.* **2009**, *38*, 1380.

(5) (a) Maji, T. K.; Mostafa, G.; Matsuda, R.; Kitagawa, S. *J. Am. Chem. Soc.* **2005**, *127*, 17152. (b) Zeng, M.-H.; Hu, S.; Chen, Q.; Xie, G.; Shuai, Q.; Gao, S.-L.; Tang, L.-Y. *Inorg. Chem.* **2009**, *48*, 7070.

(6) (a) Biradha, K.; Hongo, Y.; Fujita, M. *Angew. Chem., Int. Ed.* **2002**, *41*, 3395. (b) Zeng, M.-H.; Feng, X.-L.; Chen, X.-M. *Dalton Trans.* **2004**, 2217. (c) Uemura, K.; Kitagawa, S.; Kondo, M.; Fukui, K.; Kitaura, R.; Chang, H.-C.; Mizutani, T. *Chem.—Eur. J.* **2002**, *8*, 3586. (d) Gurunatha, K. L.; Maji, T. K. *Inorg. Chem.* **2009**, *48*, 10886.

Published on Web 11/30/2010

Scheme 1. Strategy for the Construction of a Mixed-Spin Kagomé Network Using Triangle Secondary Building Units Consisting of $tzdc^{3-}$ and Divalent Magnetic Metal Ions

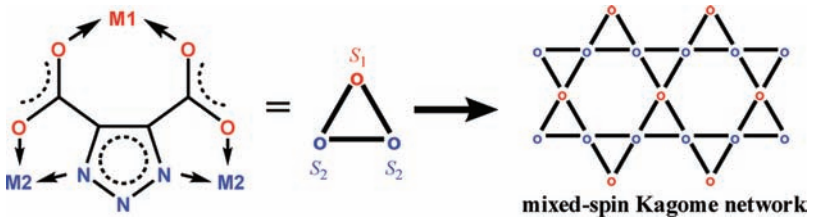

combines the porosity within the layer and/or that between the layers.[9] To date, a number of ideal or distorted homospin Kagomé systems have been synthesized with different transition metal ions such as Fe^{3+}, Cu^{2+}, Mn^{2+}, V^{3+}, Co^{2+}, Fe^{2+}, and Ni^{2+}.[10] However, the mixed-spin Kagomé systems, which also reveal fascinating magnetic properties, are only limited to a family of $(Co_xNi_{1-x})_3V_2O_8$ compounds,[11] three organically templated metal sulfates of $[HN(CH_2)_6NH][H_3O][Fe^{III}Fe^{II}{}_2F_6(SO_4)_2]$, $[C_4N_2H_{12}][NH_4]_2[Co_2NiF_6(SO_4)_2]$, and $[C_4N_2H_{12}][NH_4]_2[CoNi_2F_6(SO_4)_2]$, as well as a mixed-valent ion glycinate $[H_3O][Fe^{III}Fe^{II}{}_2F_8(CO_2CH_2NH_3)_2]$.[12]

For the construction of a Kagomé network, the triangular arrangement of magnetic metal centers is essential. Thus, we have employed the anionic, chelating ligand 1,2,3-triazole-4,5-dicarboxylate ($tzdc^{3-}$) to assemble some geometrical spin-frustration or spin-competing systems, including two homo-spin distorted Kagomé lattices with Mn^{2+} ions.[13] As shown in Scheme 1, $tzdc^{3-}$ has one *O*,*O*′-bidentate site and two *N*,*O*-bidentate sites, which can be expected to selectively chelate oxophilic metal ions, M1 (e.g., Mg^{2+}, Ca^{2+}, Mn^{2+}, Fe^{2+}, and Ln^{3+}), and nitrogen-favored metal ions, M2 (e.g., Cu^{2+} and Co^{2+}). Presumably, when M1 and M2 are divalent magnetic metal ions with spins of S_1 and S_2, respectively, they can be bridged by $tzdc^{3-}$ ligands in a neutral mixed-spin Kagomé network.

Herein, we report the syntheses, structures, and magnetic properties of two mixed-spin Kagomé compounds formulated as $[Cu_2M(tzdc)_2(H_2O)_2]\cdot 2H_2O$ [M = Fe^{2+} (**1**) or Mn^{2+} (**2**)], which exhibit a reversible structural transformation triggered by dehydration and rehydration, concomitant with a reversible magnetism change between a ferrimagnetic character for the hydrated samples and a suppressed ferrimagnetic character for the dehydrated samples.

Experimental Section

Materials and Methods. 1,2,3-Triazole-4,5-dicarboxylic acid (H_3tzdc) was synthesized according to the patented method.[14] All other reagents and solvents employed were commercially available and used as received without further purification.

The C, H, and N elemental analyses were conducted with a Vario EL elemental analyzer. The thermogravimetric (TG) analyses were performed on a NETZSCH TG 209 F3 thermogravimetric analyzer in flowing N_2 with a heating rate of 10 K/min. The powder X-ray diffraction (PXRD) data were collected on a Bruker D8-Advance diffractometer with Cu Kα radiation. The magnetic susceptibility data of randomly oriented powder samples were collected in the temperature range of 1.8−300 K on a Quantum Design MPMS XL-7 SQUID magnetometer. We prepared the samples of dehydrated compounds by heating their hydrated compounds at 200 °C under vacuum for 12 h and then sealed them into the sample holders for the magnetic measurements in the glovebox to avoid rehydration. All the magnetic susceptibilities were corrected by diamagnetic susceptibilities estimated from Pascal's constants.[15]

Preparation of $[Cu_2Fe(tzdc)_2(H_2O)_2]\cdot 2H_2O$ (1). A mixture of $Cu(NO_3)_2\cdot 3H_2O$ (0.240 g, 1.0 mmol), $FeCl_2\cdot 4H_2O$ (0.081 g, 0.5 mmol), $H_3tzdc\cdot 2H_2O$ (0.192 g, 1.0 mmol), NaOH (0.06 g, 1.5 mmol), and H_2O (7 mL) was put into a 15 mL Teflon-lined stainless autoclave and heated at 160 °C for 3 days, followed by slow cooling (0.1 °C/min) to room temperature. The dark-green block crystals of **1** were collected in a yield of 55% (0.310 g). Anal. Calcd for $C_8H_8Cu_2FeN_6O_{12}$: C, 17.06; H, 1.43; N, 14.92. Found: C, 17.10; H, 1.62; N, 15.12.

(7) (a) Kitaura, R.; Seki, K.; Akiyama, G.; Kitagawa, S. *Angew. Chem., Int. Ed.* **2003**, *42*, 428. (b) Kondo, A.; Noguchi, H.; Ohnishi, S.; Kajiro, H.; Tohdoh, A.; Hattori, Y.; Xu, W.-C.; Tanaka, H.; Kanoh, H.; Kaneko, K. *Nano Lett.* **2006**, *6*, 2581. (c) Kondo, A.; Noguchi, H.; Carlucci, L.; Proserpio, D. M.; Ciani, G.; Kajiro, H.; Ohba, T.; Kanoh, H.; Kaneko, K. *J. Am. Chem. Soc.* **2007**, *129*, 12362.

(8) (a) Takaoka, K.; Kawano, M.; Tominaga, M.; Fujita, M. *Angew. Chem., Int. Ed.* **2005**, *44*, 2151. (b) Takaoka, K.; Kawano, M.; Hozumi, T.; Ohkoshi, S.; Fujita, M. *Inorg. Chem.* **2006**, *45*, 3976.

(9) (a) Pati, S. K.; Rao, C. N. R. *Chem. Commun.* **2008**, 4683. (b) Pati, S. K.; Rao, C. N. R. *J. Chem. Phys.* **2005**, *123*, 234703.

(10) For example: (a) Grohol, D.; Nocera, D. G. *J. Am. Chem. Soc.* **2002**, *124*, 2640. (b) Papoutsakis, D. G.; Grohol, D.; Nocera, D. G. *J. Am. Chem. Soc.* **2002**, *124*, 2647. (c) Nocera, D. G.; Bartlett, B. M.; Grohol, D.; Papoutsakis, D.; Shores, M. P. *Chem.—Eur. J.* **2004**, *10*, 3850. (d) Shores, M. P.; Nytko, E. A.; Bartlett, B. M.; Nocera, D. G. *J. Am. Chem. Soc.* **2005**, *127*, 13462. (e) Helton, J. S.; Matan, K.; Shores, M. P.; Nytko, E. A.; Bartlett, B. M.; Yoshida, Y.; Takano, Y.; Qiu, Y.; Chung, J.-H.; Nocera, D. G.; Lee, Y. S. *Phys. Rev. Lett.* **2007**, *98*, 107204. (f) Nytko, E. A.; Helton, J. S.; Müller, P.; Nocera, D. G. *J. Am. Chem. Soc.* **2008**, *130*, 2922. (g) Zheng, Y.-Z.; Tong, M.-L.; Zhang, W.-X.; Chen, X.-M. *Chem. Commun.* **2006**, 165. (h) Behera, J. N.; Rao, C. N. R. *J. Am. Chem. Soc.* **2006**, *128*, 9334. (i) Kanoo, P.; Madhu, C.; Mostafa, G.; Maji, T. K.; Sundaresan, A.; Pati, S. K.; Rao, C. N. R. *Dalton Trans.* **2009**, 5062.

(11) (a) Qureshi, N.; Fuess, H.; Ehrenberg, H.; Hansen, T. C.; Ritter, C.; Prokes, K.; Podlesnyak, A.; Schwabe, D. *Phys. Rev. B* **2006**, *74*, 212407. (b) Zhang, Q.; Knafo, W.; Grubea, K.; Löhneysena, H. V.; Meingast, C.; Wolf, T. *Phys. B* (*Amsterdam, Neth.*) **2008**, *403*, 1404. (c) Qureshi, N.; Fuess, H.; Ehrenberg, H.; Hansen, T. C.; Ritter, C.; Adelmann, P.; Meingast, C.; Wolf, T.; Zhang, Q.; Knafo, W. *J. Phys.: Condens. Matter* **2008**, *20*, 095219. (d) Qureshi, N.; Fuess, H.; Ehrenberg, H.; Ouladdiaf, B.; Rodríguez-Carvajal, J.; Hansen, T. C.; Wolf, T.; Meingast, C.; Zhang, Q.; Knafo, W.; Löhneysena, H. V. *J. Phys.: Condens. Matter*. **2008**, *20*, 235228.

(12) (a) Paul, G.; Choudhury, A.; Sampathkumaran, E. V.; Rao, C. N. R. *Angew. Chem., Int. Ed.* **2002**, *41*, 4297. (b) Rao, C. N. R.; Paul, G.; Choudhury, A.; Sampathkumaran, E. V.; Raychaudhuri, A. K.; Ramasesha, S.; Rudra, I. *Phys. Rev. B* **2003**, *67*, 134425. (c) Nagaraja, C. M.; Behera, J. N.; Maji, T. K.; Pati, S. K.; Rao, C. N. R. *Dalton Trans.* **2010**, *39*, 6947. (d) Dan, M. *J. Mol. Struct.* **2004**, *706*, 127.

(13) (a) Shi, W.; Chen, X.-Y.; Xu, N.; Song, H.-B.; Zhao, B.; Cheng, P.; Liao, D.-Z.; Yan, S.-P. *Eur. J. Inorg. Chem.* **2006**, *23*, 4931. (b) Yue, Y.-F.; Wang, B.-W.; Gao, E.-Q.; Fang, C.-J.; He, C.; Yan, C.-H. *Chem. Commun.* **2007**, 2034. (c) Zhang, W.-X.; Xue, W.; Lin, J.-B.; Zheng, Y.-Z.; Chen, X.-M. *CrystEngComm* **2008**, *10*, 1770. (d) Zhang, W.-X.; Xue, W.; Zheng, Y.-Z.; Chen, X.-M. *Chem. Commun.* **2009**, 3804. (e) Yue, Y.-F.; Liang, J.; Gao, E.-Q.; Fang, C.-J.; Yan, Z.-G.; Yan, C.-H. *Inorg. Chem.* **2008**, *47*, 6115.

(14) Suverkropp, G. H.; Alsters, P. L.; Snijder, C. S.; De Vries, J. G. U.S. Patent 5917049, 1999.

(15) Mabbs, F. E.; Machin, D. J. *Magnetism and Transition Metal Complexes*; Chapman and Hall: London, 1973.

Table 1. Crystallographic Data for **1** and **2**

	1	**2**
empirical formula	$C_8H_8Cu_2FeN_6O_{12}$	$C_8H_8Cu_2MnN_6O_{12}$
formula weight	563.13	562.22
crystal system	monoclinic	monoclinic
space group	$C2/m$	$C2/m$
T (K)	293(2)	293(2)
a (Å)	7.336(2)	7.390(1)
b (Å)	12.020(2)	12.016(2)
c (Å)	8.670(2)	8.754(1)
β (deg)	104.213(3)	104.409(2)
V (Å^3)	741.1(2)	752.8(2)
D_c (g/cm^3)	2.524	2.48
Z	2	2
μ (mm^{-1})	3.901	3.715
no. of reflections collected	1712	1836
no. of unique reflections	765	777
R_{int}	0.0183	0.0143
goodness of fit on F^2	1.117	1.316
R_1[a] $[I > 2\sigma(I)]$	0.0262	0.0383
wR_2[b] (all data)	0.0715	0.0863
$\Delta\rho_{max}/\Delta\rho_{min}$ (e/Å^3)	0.462/−0.345	0.645/−1.691

[a] $R_1 = \sum||F_o| - |F_c||/\sum|F_o|$. [b] $wR_2 = [\sum w(F_o^2 - F_c^2)^2/\sum w(F_o^2)^2]^{1/2}$, and $w = (\sigma^2(F_o^2)^2 + \{0.1[\max(0,F_o^2) + 2F_c^2]/3\}^2)^{-1}$.

Preparation of $[Cu_2Mn(tzdc)_2(H_2O)_2]\cdot 2H_2O$ (2). 2 was synthesized in a manner analogous to that of **1** by using $MnCl_2\cdot 4H_2O$ (0.099 g, 0.5 mmol) in place of $FeCl_2\cdot 4H_2O$. The green block crystals of **2** were collected after being washed with water with a yield of 50% (0.281 g). Anal. Calcd for $C_8H_8Cu_2MnN_6O_{12}$: C, 17.09; H, 1.43; N, 14.95. Found: C, 17.11; H, 1.48; N, 14.97.

X-ray Crystallography. The single-crystal diffraction data of **1** and **2** were collected on a Bruker Smart Apex CCD diffractometer with graphite-monochromatized Mo Kα radiation (λ = 0.71073 Å) at 293(2) K. All intensity data were corrected for Lorentz and polarization effects, and absorption corrections were applied by using the multiscan program SADABS. The structures were determined by direct methods and refined by the full-matrix least-squares method on F^2 with SHELXTL.[16] All non-hydrogen atoms were refined with anisotropic displacement parameters. The organic hydrogen atoms were generated geometrically. Crystal data as well as details of data collection and refinements for **1** and **2** are summarized in Table 1. Selected bond distances and bond angles are listed in Table 3.

The PXRD data of **1′** and **2′** were collected via Bruker D8 Advance with Cu Kα X-ray radiation (40 kV, 40 mA) at 503(2) K. The indexes were derived with JADE, and Pawley refinements following the space group analysis were performed with the Reflex plus module of Material Studio, showing the symmetries of the new phases have not changed. Therefore, space group $C2/m$ was selected for both **1′** and **2′**, and the structural models without the water molecules of **1** and **2** were used as the initial structural models for the Rietveld refinements of **1′** and **2′**, respectively, which were performed with the Reflex plus module of Material Studio. The data collection and refinement statistics for **1′** and **2′** are listed in the Supporting Information and summarized in Table 2. Selected bond distances and bond angles are listed in Table 3.

Results and Discussion

Crystal Structures of 1 and 2. Single-crystal X-ray analysis reveals that **1** and **2** are isomorphous and crystallize in monoclinic space group $C2/m$ with the asymmetrical units consisting of one Cu^{2+} ion and one M^{2+} ion. Taking **1** as an example (Figure 1a), we find the octahedral Fe1 atom, being located at an inversion center and in a minor plane, is chelated by two O,O'-bidentate sites of $tzdc^{3-}$ at the equatorial positions [Fe1−O2, 2.112(2) Å], as expected, while its axial positions are occupied by two water molecules [Fe1−O1W, 2.103(3) Å]. Being located at an inversion center in an elongated 4+2 coordination geometry, Cu1 is chelated by two N,O-bidentate sites of $tzdc^{3-}$ at the equatorial positions [Cu1−O1, 1.975(2) Å; Cu1−N1, 1.957(2) Å], and two oxygen atoms are very weakly coordinated at its axial positions [Cu1···O1F, 2.792(2) Å]. The $tzdc^{3-}$ ligand with a μ_3-bridging mode, being located in a minor plane, chelates two Cu^{2+} ions with N,O-bidentate sites and one Fe^{2+} ion with an O,O'-bidentate site, which further link these ions into flat layers with Kagomé magnetic topology in the (201) crystallographic plane (Figure 1b). These layers furnish microcavities enclosed by six $tzdc^{3-}$ ions and six metal ions, which are occupied by two coordinated water molecules and two lattice water molecules involving hydrogen bonding interactions (see Figure S2 of the Supporting Information).

(16) *SHELXTL*, version 6.10; Bruker Analytical Instrumentation: Madison, WI, 2000.

Table 2. Crystallographic Data for **1′** and **2′**

	1′	**2′**
empirical formula	$C_8Cu_2FeN_6O_8$	$C_8Cu_2MnN_6O_8$
formula weight	491.06	490.15
crystal system	monoclinic	monoclinic
space group	$C2/m$	$C2/m$
T (K)	503(2)	503(2)
a (Å)	7.073(2)	7.091(4)
b (Å)	12.245(4)	12.198(6)
c (Å)	7.458(3)	7.592(4)
β (deg)	118.475(6)	118.367(4)
V (Å^3)	567.8(3)	577.8(5)
D_c (g/cm^3)	2.872	2.817
Z	2	2
R_p[a]	1.19%	1.66%
R_{wp}[b]	2.07%	2.75%

[a] $R_p = \sum|cY^{sim}(2\theta_i) - I^{exp}(2\theta_i) + Y^{back}(2\theta_i)|/\sum|I^{exp}(2\theta_i)|$. [b] $R_{wp} = \{w[cY^{sim}(2\theta_i) - I^{exp}(2\theta_i) + Y^{back}(2\theta_i)]^2/\sum w[I^{exp}(2\theta_i)]^2\}^{1/2}$, and $w = 1/I^{exp}(2\theta_i)$.

Table 3. Selected Interatomic Distances (angstroms), Bond Angles (degrees), and Torsion Angles (degrees) for **1**, **2**, **1′**, and **2′**[a]

	1	**2**	**1′**	**2′**
M1−O2	2.112(2)	2.154(3)	2.009(5)	2.033(5)
M1−O1W	2.103(3)	2.161(4)	−	−
M1···N2F	3.973(3)	4.006(4)	2.751(3)	2.872(3)
Cu1−N1	1.957(2)	1.955(3)	1.963(1)	1.952(1)
Cu1−O1	1.975(2)	1.976(3)	2.023(5)	2.005(6)
Cu1···O1F	2.792(2)	2.807(3)	2.972(4)	2.759(5)
O2−M1−O2A	96.7(1)	94.8(1)	82.3(1)	82.5(1)
O2−M1−O1W	90.0(1)	90.1(1)	−	−
O2−M1−N2F	−	−	84.6(1)	84.0(1)
N1−Cu1−O1	82.5(1)	82.5(1)	86.4(1)	88.4(1)
O1−Cu1−O1F	80.7(1)	80.2(1)	91.8(1)	85.0(2)
N1−Cu1−O1F	90.5(1)	91.5(1)	92.6(1)	95.0(1)
N1−C2−C1−O1	2.1(3)	2.5(5)	−3.9(4)	3.8(4)
Cu1···Cu1A	6.010(1)	6.0080(8)	6.123(2)	6.099(3)
Cu1···Cu1F	3.6681(7)	3.6947(5)	3.537(1)	3.546(2)
Cu1···M1	5.9236(7)	5.9682(5)	5.718(1)	5.766(2)
Cu1−O1−Cu1F	99.2(1)	99.7(1)	88.0(2)	94.9(2)
Cu1−O1−C1	115.2(2)	115.1(2)	106.8(1)	106.9(1)
M1−O2−C1	140.8(2)	141.7(2)	144.9(1)	143.9(1)
Cu1−O1−C1−O2	177.(2)	176.8(3)	174.3(3)	177.5(3)
M1−O2−C1−O1	179.5(2)	180.0(3)	138.6(5)	133.2(5)

[a] M = Fe^{2+} for **1** and **1′**, and M = Mn^{2+} for **2** and **2′**. Symmetry codes: (A) $x, -y, z$; (F) $-x, y, -z$.

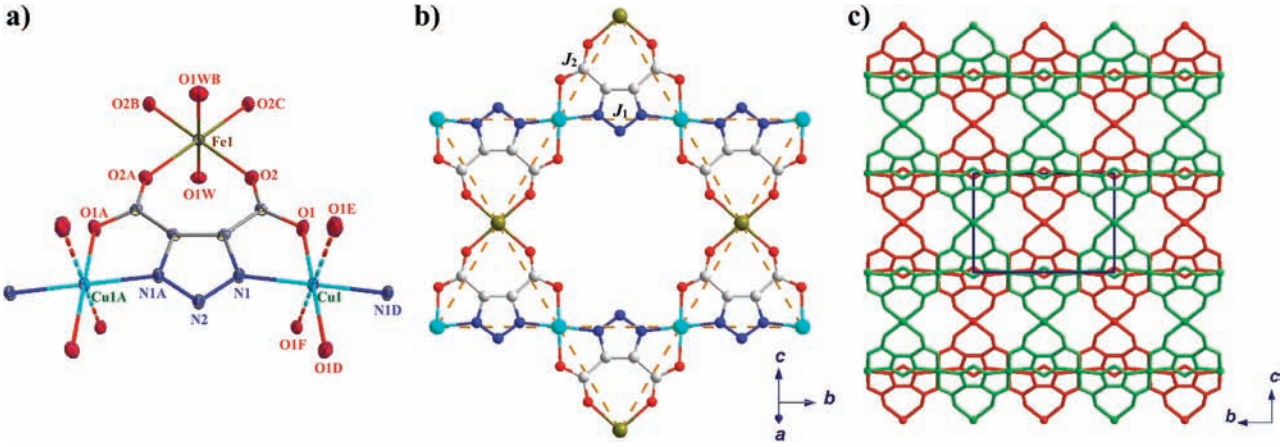

Figure 1. (a) Asymmetrical unit of **1** in an ORTEP view (50% thermal ellipsoids). (b) Kagomé layer consisting of $tzdc^{3-}$ and metal ions (the dashed line between the metal ions presents the Kagomé magnetic exchange topology). (c) AB packing mode of these layers viewed along the *a* axis. The adjacent layers are colored red and green, respectively, and the water molecules have been omitted for the sake of clarity. Symmetry codes: (A) $x, -y, z$; (B) $-x, -y, -z+1$; (C) $-x, y, -z+1$; (D) $-x+{}^1/_2, -y+{}^1/_2, -z$; (E) $x+{}^1/_2, -y+0.5, z$; (F) $-x, y, -z$.

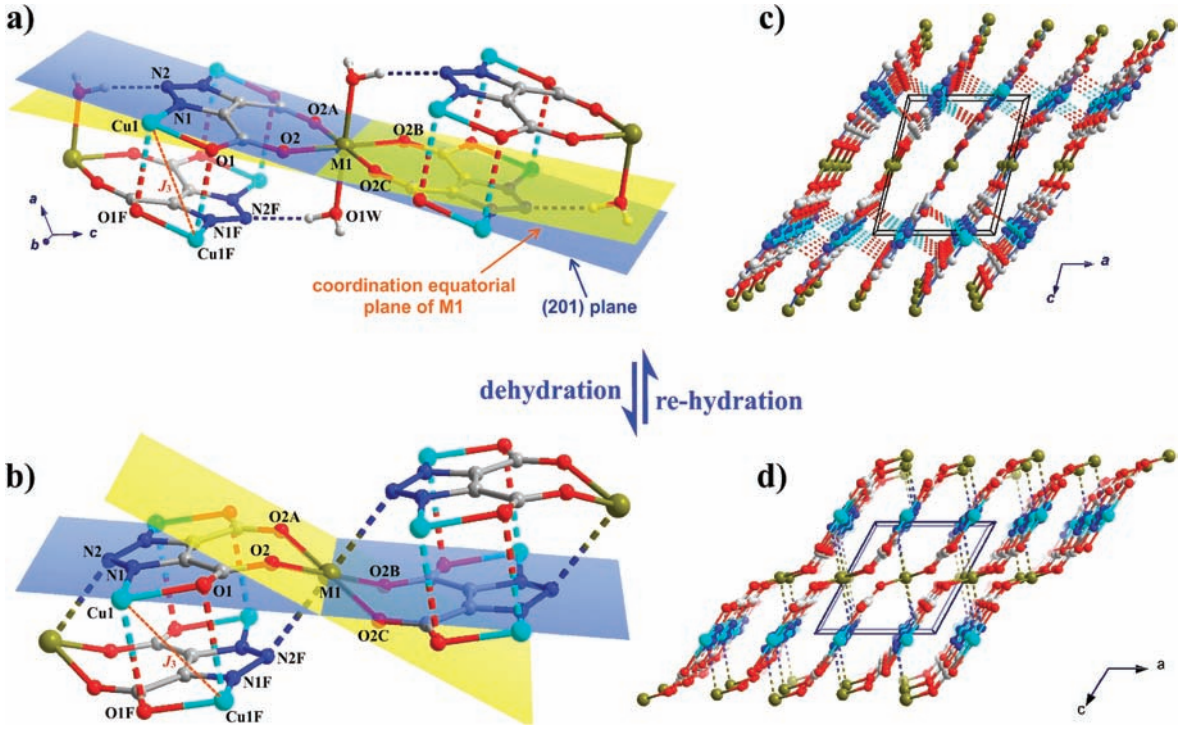

Figure 2. (a and b) Coordination sphere of M1 and corresponding structural changes during dehydration and rehydration. (c and d) Packing of the Kagomé layers viewed along the *b* axis. The water molecules have been omitted for the sake of clarity. Symmetry codes: (A) $x, -y, z$; (B) $-x, -y, -z+1$; (C) $-x, y, -z+1$; (F) $-x, y, -z$.

These layers are further packed into a three-dimensional structure along the *a* axis in an AB packing mode (Figure 1c) with weak interlayer Cu···O coordination (Figure 2a,c) and hydrogen bonding interactions involving the water molecules. For **2**, the coordination bond lengths are very similar to those of **1**, except the Mn−O bonds are slightly longer [Mn1−O2, 2.154(3) Å; Mn1−O1W, 2.161(4) Å], which is caused by the radius of the Mn^{2+} ion being longer than that of the Fe^{2+} ion.

Thermogravimetric Analysis. Thermogravimetric analyses of both **1** and **2** show two-step weight losses in the range of 100−200 and 200−300 °C (see Figure S3 of the Supporting Information), which correspond to the release of two uncoordinated water molecules and two coordinated water molecules (calcd 6.4 and 6.4 wt % for **1** and 6.4 and 6.4 wt % for **2**; found 6.8 and 6.6 wt % for **1** and 6.4 and 6.3 wt % for **2**), respectively. The PXRD patterns of **1** and **2** at different temperatures (see Figure S4 of the Supporting Information) indicate that two new phases (**1′** and **2′**) are formed after the coordinated water molecules are removed. Both **1′** and **2′** can be stable up to ca. 300 °C and can be recovered by the quick reabsorption of H_2O molecules when they are exposed to air. The TGA plots and PXRD patterns of these rehydrated samples are almost identical to those of the original hydrate samples (see Figure S5 of the Supporting Information), indicating

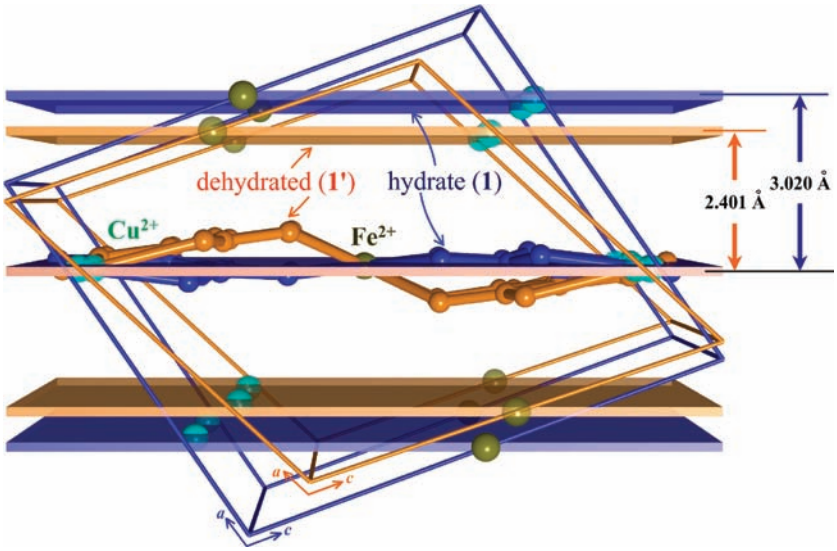

Figure 3. Comparison between the cells, (201) planes, and atom positions of **1** (blue) and **1′** (orange) viewed along the *b* axis, by overlapping their (201) planes passing through the center of the cell.

that **1** and **2** are flexible and can exhibit reversible structural transformations in response to the release and readsorption of water molecules.

Structures of Dehydrated Phases 1′ and 2′. The structures derived from PXRD patterns (see the Supporting Information) reveal that **1′** and **2′** are isomorphous, which also crystallize in the *C*2/*m* space group and exhibit 2D Kagomé layers with an AB packing mode like the original hydrated phases. However, as shown in Figure 2b, the coordination sphere of M^{2+} is changed from an octahedron to an elongated 4+2 octahedral form. Its four equatorial positions are also occupied by two $tzdc^{3-}$ ions with the *O*,*O*′-bidentate mode [Fe1−O2, 2.009(5) Å; Mn1−O2, 2.033(5) Å], while the axial positions are now occupied by two triazolate N atoms from adjacent layers with very weak coordination interactions [Fe1−N2F, 2.751(3) Å; Mn1−N2F, 2.872(3) Å] instead of the water molecules in the hydrate phase. The atoms of the $tzdc^{3-}$ anion are kept coplanar, which is consistent with the π_{11}^{14} conjugated bond of the $tzdc^{3-}$ anion determined by a previous DFT calculation.[13a] However, to fit the coordination sphere changes of M1 ions, the $tzdc^{3-}$ anions rotate slightly along the axis passing through Cu1 and Cu1A, causing an evident deviation of the carboxylate groups from the (201) plane (Figures 2b,d and 3). Accordingly, the dihedral angle between the Kagomé layer and the coordination equatorial plane of the M^{2+} ion changes drastically from −5.77(5)° to 24.9(1)° for **1′** and from −5.31(6)° to 22.7(1)° for **2′**, and the intralayer Cu1···M1 distance is slightly reduced from 5.9236(7) to 5.718(1) Å for **1′** and from 5.9682(5) to 5.766(2) Å for **2′**. Meanwhile, the distance between the adjacent Kagomé layers is reduced drastically from 3.02 to 2.40 Å for **1′** and from 3.04 to 2.42 Å for **2′** (Figure 3). This fact indicates that, upon the release of water molecules, the Kagomé layers become remarkably wrinkled along the [$\bar{1}$02] direction and are packed more closely to eliminate the void (ca. 13.3 and 15.3% of the total crystal volumes for **1** and **2**, respectively) occupied by the water molecules in the hydrated phases,[17] leading to the increase in density from 2.524 to 2.872 g/cm^3 for **1′** and from 2.480 to 2.817 g/cm^3 for **2′**.

Although a few dynamic 2D microporous coordination polymers showing structural transformations triggered by the release and/or readsorption of guest and/or coordination molecules have been documented,[4−8] the soft layered coordination polymers showing the considerable intralayer distortion (Figure 4c) are still rare upon comparison with those rigid 2D ones revealing the interlayer structural changes, including the parallel-layer and/or perpendicular-layer sliding (Figure 4a,b).[6,7] To the best of our knowledge, only two isomorphic Co^{2+} and Ni^{2+} square-grid networks were reported to exhibit the considerable intralayer distortion rather than the interlayer sliding triggered by a ligand-exchange reaction between H_2O and NO_3^-.[8] Compared to these analogues, isomorphic **1** and **2** are more flexible, as they can exhibit not only a considerable intralayer wrinkling but also a remarkable interlayer superimposition, leading to a reversible structural transformation from microporous to nonporous structures, as well as a reversible change in magnetism (vide infra).

Magnetic Properties. The temperature-dependent magnetic susceptibilities of the four compounds are shown in Figure 5. The $\chi_m T$ value of **1** is 4.04 cm^3 mol^{-1} K at 300 K, slightly larger than the spin-only value (3.75 cm^3 mol^{-1} K) of two isolated Cu^{2+} ions and one high-spin Fe^{2+} ion because of the orbital contribution of Fe^{2+} ions.[18] When the temperature is decreased, the $\chi_m T$ decreases slowly to 12 K and then increases to the maximum value (6.55 cm^3 mol^{-1} K) before decreasing again. For **2**, its $\chi_m T$ value at 300 K is 4.89 cm^3 mol^{-1} K, being slightly less than the spin-only value (5.125 cm^3 mol^{-1} K) of two isolated Cu^{2+} ions and one high-spin Mn^{2+} ion. When the temperature decreases, its $\chi_m T$ value decreases slowly to 4.17 cm^3 mol^{-1} K (at 26 K) and then increases to 5.52 cm^3 mol^{-1} K

(17) Spek, L. *PLATON, A Multipurpose Crystallographic Tool*; Utrecht University: Utrecht, The Netherlands, 2001.

(18) (a) Carlin, R. L. *Magnetochemistry*; Springer-Verlag: New York, 1981. (b) Kahn, O. *Molecular Magnetism*; VCH: New York, 1993.

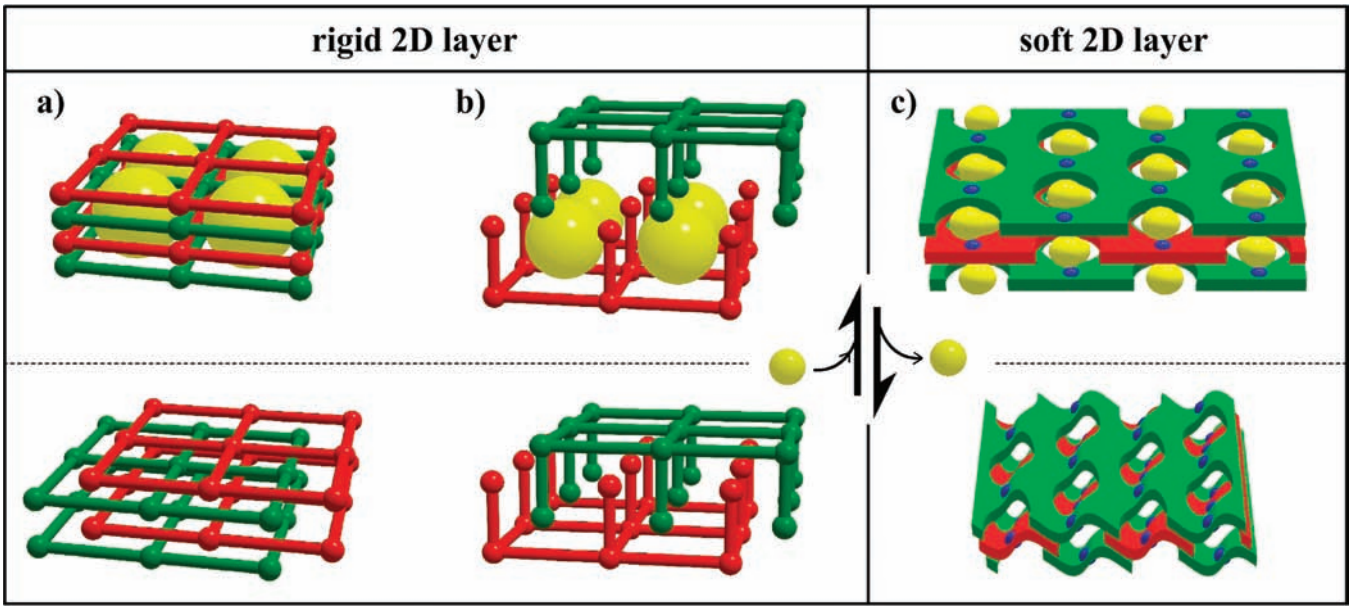

Figure 4. Schematic presentations for the known dynamic structural transformations of 2D networks (red and green skeleton or plane) triggered by release and/or resorption of the uncoordinated and/or coordinated molecules (yellow spheres). For the rigid 2D layers, the structural changes mainly come from parallel-layer sliding (a)[6] or perpendicular-layer superimposition (b).[7] For the soft 2D layers, their structural flexibility can come from both intralayer distortion and the interlayer structural changes (c), which is demonstrated here by **1** and **2**.

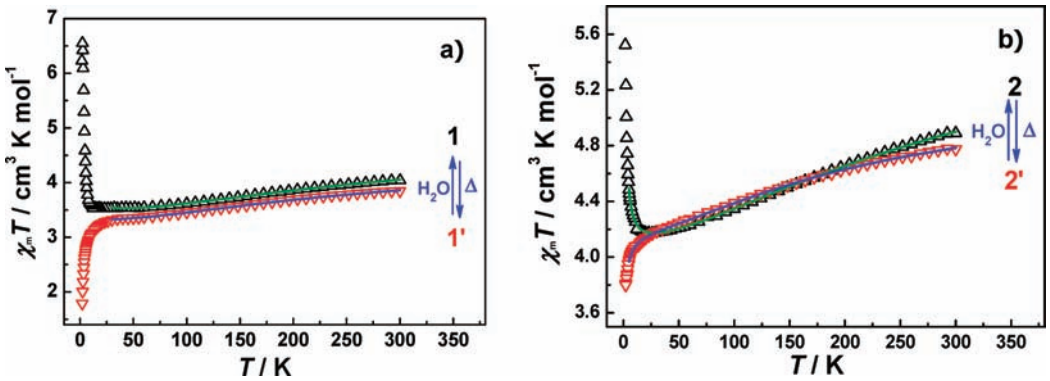

Figure 5. Temperature-dependent DC magnetic susceptibilities of **1**, **2**, **1′**, and **2′**. The solid lines represent the best-fit curves (see the text and the Supporting Information).

(at 1.8 K). The data of **1** and **2** between 300 and 100 K were fitted by the Curie−Weiss law (see Figure S6 of the Supporting Information), leading to the following parameters: for **1**, $C = 4.33(2)$ cm^3 mol^{-1} K and $\theta = -23.0(9)$ K, and for **2**, $C = 5.25(3)$ cm^3 mol^{-1} K and $\theta = -24.0(9)$ K. The negative Weiss constants indicate antiferromagnetic coupling dominating these systems.[18] Therefore, the typical ferrimagnetic behaviors of **1** and **2** should be ascribed to the incomplete cancellation of antiferromagnetic coupling between Cu^{2+} and Fe^{2+}/Mn^{2+} ions through the anti-anti carboxylate bridges within the mixed-spin Kagomé layers. Furthermore, no magnetic long-range ordering or spin-glass behaviors were found above 1.8 K for **1** and **2** (see Figures S7−S9 of the Supporting Information).[19] By employing quantum many-body Heisenberg models, Pati and Rao[9b] have found that the mixed-spin Kagomé system would theoretically behave as a classical magnet with a ferrimagnetic ground state showing weak or the near absence of the spin frustration, especially when $S_1 > 2S_2$. Indeed, the reported mixed-valent iron Kagomé complexes and mixed-metal sulfates reveal experimentally the typical classical magnetic behavior,[12] and in the case presented here, both **1** and **2** also reveal notable ferrimagnetic character, although no long-range ordering was observed above 1.8 K. Furthermore, compared with the reported mixed-spin Kagomé systems, **1** and **2** have more complicated magnetic properties in that they exhibit the reversible magnetism driven by the release and/or rebonding of the water molecules coordinated to the Fe^{2+}/Mn^{2+} ions.

As shown in Figure 5, the $\chi_m T$ values of dehydrated **1′** and **2′** are 3.85 and 4.77 cm^3 mol^{-1} K, respectively, at 300 K, and slightly lower than those of their hydrate phases, which should be mainly ascribed to the coordination sphere changes of Fe^{2+}/Mn^{2+} ions. The Curie−Weiss

(19) Both the real and imaginary parts of AC magnetic susceptibilities of **1** and **1′** reveal a slight frequency-dependent signal at ca. 2 K (Figure S8 of the Supporting Information); however, the spin-glass-like behavior was precluded by the zero-field-cooled magnetization and field-cooled magnetization [ZFCM-FCM (Figure S9 of the Supporting Information)] of **1** and the hystersis plots of **1** and **1′** (Figure S7a of the Supporting Information). Such a slight frequency-dependent signal should be caused by a slight impurity in these samples produced during hydrothermal synthesis.

law fitting in the range of 100−300 K gives the following parameters: for **1′**, $C = 4.12(4)$ cm^3 mol^{-1} K and $\theta = -22.1(8)$ K, and for **2′**, $C = 5.03(1)$ cm^3 mol^{-1} K and $\theta = -16.4(5)$ K (Figure S6 of the Supporting Information). It is noteworthy that the $\chi_m T$ values of **1′** and **2′** continuously decrease upon cooling and reach 1.79 and 3.80 cm^3 mol^{-1} K at 2.0 K, respectively. The absence of peaks in the $\chi_m T$ curves above 2.0 K implies that the ferrimagnetic behavior is suppressed after dehydration, which is further confirmed by the slower increase in the field-dependent magnetizations of dehydrated samples than those of original hydrate samples at low fields (Figure S7 of the Supporting Information).

Obviously, a precise theoretical treatment of magnetic properties for these compounds cannot be conducted because there are three kinds of magnetic coupling with different magnitudes: J_1 stands for the triazolate bridge between Cu1 and Cu1A, J_2 stands for the anti-anti carboxylate bridge between Cu1 and Fe1/Mn1, and J_3 stands for the magnetic coupling passed through weakly coordinated oxygen atom O1F between Cu1 and Cu1A. However, it has been realized that the triazolate bridges of tzdc^{3-} can transmit strong antiferromagnetic coupling (−139 cm^{-1}) for Cu^{2+} ions,[13b] the anti-anti carboxylate bridges transmit the antiferromagnetic coupling with a typical value on the order of −10 cm^{-1},[20] and the magnetic coupling J_3 passed via the weak coordination interactions is negligible compared with J_1 and J_2.[21] Therefore, we could roughly estimate the magnetic coupling interactions J_1 by assuming that the total magnetic susceptibility χ_{tol} is given by the sum of the antiferromagnetic Cu^{2+} chains and paramagnetic contribution of the isolated Fe^{2+}/Mn^{2+} ions (eqs 1−3).[18,22]

$$\chi_{tol} = 2\chi_{Cu\text{-}chain} + \chi_M \tag{1}$$

$$\chi_{Cu\text{-}chain} = \frac{Ng_{Cu}{}^2\beta^2}{kT}\frac{0.25 + 0.074975x + 0.075235x^2}{1.0 + 0.9931x + 0.172135x^2 + 0.757825x^3}$$
$$x = |J_1|/kT \tag{2}$$

$$\chi_M = N\beta^2 g_M{}^2 S_M(S_M+1)/3kT$$
$$[M = \text{Fe (}\mathbf{1}\text{ and }\mathbf{1}'\text{) or Mn (}\mathbf{2}\text{ and }\mathbf{2}'\text{)}] \tag{3}$$

where g_{Cu} and g_M are g-factors of Cu^{2+} and Fe^{2+}/Mn^{2+} ions, respectively, N is Avogadro's number, β is the Bohr magneton, and k is the Boltzmann constant. Then a correction item θ' was included to mainly account for the effect of magnetic interaction occurring between the Cu^{2+} chains and Fe^{2+}/Mn^{2+} ions, and a parameter N_a was included to account for the temperature-independent paramagnetic susceptibilities, which results in eq 4.

$$\chi = \frac{\chi_{tol}T}{T-\theta'} + N_a \tag{4}$$

To avoid deviation of eq 4 by the interlayer magnetic interaction and the zero-field-splitting effect of Fe^{2+} ions, only the data above 30 K were fitted for **1** and **1′** by the least-squares method, leading to the following parameters: for **1**, $g_{Cu} = 2.0$ (fixed),[23] $g_{Fe} = 2.11(1)$, $J_1 = -195(7)$ cm^{-1}, $\theta' = 1.1(1)$ K, $N_a = 8.7(2) \times 10^{-4}$ cm^3 mol^{-1}, and $R = 2.2 \times 10^{-6}$ [$R = \sum(\chi_{obs}T - \chi_{calc}T)^2/\sum(\chi_{calc}T)^2$], and for **1′**, $g_{Cu} = 2.0$ (fixed), $g_{Fe} = 2.07(1)$, $J_1 = -182(6)$ cm^{-1}, $\theta' = 0.5(1)$ K, $N_a = 6.3(2) \times 10^{-4}$ cm^3 mol^{-1}, and $R = 1.8 \times 10^{-6}$. For **2** and **2′**, the data above 5 K were fitted with the following parameters: for **2**, $g_{Cu} = 2.0$ (fixed), $g_{Mn} = 1.92(1)$, $J_1 = -174(4)$ cm^{-1}, $\theta' = 0.51(1)$ K, $N_a = 1.38 \times 10^{-3}$ cm^3 mol^{-1}, and $R = 2.6 \times 10^{-6}$, and for **2′**, $g_{Cu} = 2.0$ (fixed), $g_{Mn} = 1.95(1)$, $J_1 = -151(2)$ cm^{-1}, $\theta' = -0.26(1)$ K, $N_a = 4.7(1) \times 10^{-4}$ cm^3 mol^{-1}, and $R = 1.2 \times 10^{-6}$. It should be point out that the positive θ' does not mean the ferromagnetic interactions between Cu^{2+} and Fe^{2+}/Mn^{2+} ions but should be ascribed to the net magnetic moment of ferrimagnetic interaction between Cu^{2+} and Fe^{2+}/Mn^{2+} ions.

A few parameters obtained from this fitting are outside the normal range, which implies such a model is too simple for the magnetic properties of these compounds. In principle, one could realize that the magnetic coupling J_1 is the dominating magnetic interaction, and it is slightly weaker after dehydration, which is consistent with the slight change in Cu1···Cu1A distances during dehydration and rehydration. By contrast, the magnitude of correct item θ' is reduced by half after dehydration, which means the magnetic susceptibilities of dehydrated compounds are much closer to the sum of the antiferromagnetic Cu^{2+} chains and the paramagnetic Fe^{2+}/Mn^{2+} ions, implying the magnetic coupling J_2 becomes much weaker after dehydration. To date, the magneto-structural correlation of the anti-anti carboxylate bridge, especially for the case of the heterometal magnetic coupling, is still limited compared with those of the syn-syn and syn-anti carboxylate bridges.[20] However, a DFT study[24] found that the deviation of Cu^{2+} ions from the carboxylate plane could cause a reduction in the antiferromagnetic coupling in a carboxylate-bridged dinuclear Cu^{2+} complex. In our case, the Cu1−O1−C1−O2 torsion angles are almost unchanged after dehydration while the M1−O1−C1−O2 torsion angles decrease from 179.5(2)° to 138.6(5)° for **1′** and from 180.0(3)° to 133.2(5)° for **2′** (Figure 2b). In other words, a remarkable deviation of Fe^{2+}/Mn^{2+} ions from the carboxylate plane was found after dehydration, which should be the main reason for the decrease in J_2 observed from the magnetic fitting. Therefore, although it is weaker than J_1, the antiferromagnetic coupling J_2 between spins S_1

(20) (a) Inoue, M.; Kubo, M. *Inorg. Chem.* **1970**, *9*, 2310. (b) Colacio, E.; Domínguez-Vera, J. M.; Ghazi, M.; Kivekäs, R.; Kling, M.; Moreno, J. M. *Eur. J. Inorg. Chem.* **1999**, 441. (c) Wang, X.-Y.; Wei, H.-Y.; Wang, Z.-M.; Chen, Z.-D.; Gao, S. *Inorg. Chem.* **2005**, *44*, 572. (d) Angaridis, P.; Kampf, J. W.; Pecoraro, V. L. *Inorg. Chem.* **2005**, *44*, 3626.

(21) The superexchange path in CuO_2Cu systems requires covalent bonding between copper and bridging oxygen atoms, where the Cu−O bond usually is shorter than 2.25 Å. In our case, the Cu···O distances are in the range of 2.759(5)−2.972(4) Å; thus, the interlayer magnetic interactions J_3 should be negligible when compared with intralayer magnetic interactions J_1 and J_2. For the magneto-structural correlation for CuO_2Cu systems, please see: Chandramouli, G. V. R.; Kundu, T. K.; Manoharan, P. T. *Aust. J. Chem.* **2003**, *56*, 1239.

(22) Estes, W. E.; Gavel, D. P.; Hatfield, W. E.; Hodgson, D. *Inorg. Chem.* **1978**, *17*, 1415.

(23) The parameters g_{Cu} and J_1 are strongly dependent in the fitting, so we fixed g_{Cu} to be the spin-only value.

(24) Rodríguez-Fortea, A.; Alemany, P.; Alvarez, S.; Ruiz, E. *Chem.—Eur. J.* **2001**, *7*, 627.

and S_2 in **1** and **2** should be comparable to the J_1 between S_2 spins (Cu^{2+} ions) and leads to the notable ferrimagnetic behavior for these hydrated compounds.[9,12] For the dehydrated compounds, however, the magnitude of J_2 is substantially reduced compared with that of J_1, leading to the suppression of the ferrimagnetic behavior of **1′** and **2′**.

Conclusion

In summary, we have successfully obtained two new mixed-spin Kagomé coordination polymers by using $tzdc^{3-}$, Cu^{2+}, and Fe^{2+}/Mn^{2+} ions, which reveal a typical ferrimagnetic character. Both uncoordinated and coordinated water molecules in these compounds can be removed upon heating. As a result, a structural transformation from the microporous to nonporous structures by the intralayer wrinkling and interlayer superimposing is found, indicating both **1** and **2** can serve as a new type of "soft" 2D framework that is different from the reported "rigid" 2D ones. Accordingly, such intralayer distortion decreases the magnetic coupling between Cu^{2+} and Fe^{2+}/Mn^{2+} ions, which results in the suppression of the ferrimagnetic character in the dehydrated samples. After the readsorption of these coordinated and guest water molecules, the structures and magnetic properties of these compounds can be recovered. Therefore, these two mixed-spin Kagomé coordination polymers presented here serve as new and unique dynamic magnets.

Acknowledgment. This work was supported by the National Science Foundation of China (20821001 and 90922031) and the "973 Program" (2007CB815302).

Supporting Information Available: Additional plots, TG analysis, magnetic data, PXRD patterns, and X-ray data files (CIF). This material is available free of charge via the Internet at http://pubs.acs.org.